Molecular Characterization of Mouse Models of High-Grade Serous Carcinoma Based on Oviductal Epithelial Transformation

Stephanie M. Schulman

Senior Honors Thesis
Cellular and Molecular Biology
April 2, 2018

Table of Contents

Abstract

Based on recent studies, the most common and lethal type of "ovarian" cancer, high grade serous carcinoma (HGSC), is thought to originate in the fallopian tube epithelium rather than from the ovarian surface epithelium [1]. To study the pathogenesis of HGSC in a mouse model, the Cho lab developed *Ovgp1-iCreER*^{T2} mice, in which the *Ovgp1* promoter is used to control expression of tamoxifen (TAM)-regulated Cre recombinase in the murine equivalent of human fallopian tube epithelium (oviductal epithelium). TAM-treated *Ovgp1-iCreER*^{T2} mice carrying various genetically engineered tumor suppressor gene alleles were used to study effects of inactivating different combinations of tumor suppressor genes in the oviductal epithelium.

Specifically, *Brca1, Trp53, Rb1,* and *Nf1* were selected because they are often inactivated in human HGSCs and lead to genetic instability and tumor development [2]. In order to characterize oviductal tumors arising in our genetically engineered mouse models and verify how comparable they are to human HGSCs, targeted exome sequencing was used to analyze the 32 most commonly mutated genes in human HGSC. Our analysis employed the sequence data to assess DNA copy number alterations (CNAs) in the mouse tumors. Unsupervised hierarchical clustering was used to group tumors based on their CNA profiles. Like human HGSCs, the mouse tumors show a high level of genomic instability, with many widely distributed CNAs. In addition, the tumors acquire other genetic changes characteristic of human HGSCs, such as amplification of c*Myc* and deletion of *Pten*.

Introduction

For women worldwide, ovarian cancer is the seventh most common cause of cancer-related death [3]. Among these cases, the most prevalent and deadly type is high-grade serous carcinoma (HGSC) [4]. While it was originally believed that the cell of origin of these cases would be found in the ovaries, research has shown that most HGSCs likely originate in the fallopian tube [5]. For this reason, the Cho lab has been studying epithelial transformation in the murine equivalent, the oviduct.

The Cho lab has generated genetically engineered mice, henceforth referred to as *Ovgp1-iCreER^{T2}* mice, in which the *Ovgp1* promoter is used to drive expression of tamoxifen-regulated Cre recombinase specifically in the oviductal epithelium [6]. When LoxP sites are placed within genes of interest, the sequence between them can be inverted, deleted or translocated depending on the orientation of the LoxP sites.

Unlike experiments using knockout mice with germline deletions, the Cre-Lox system can allow for targeted, tissue specific, inducible knockouts [7]. In our case, *Ovgp1-iCreER^{T2}* mice were crossed with mice that contained different combinations of specific Cre-inducible (floxed) tumor suppressor genes (*Trp53, Rb1, Brca1, Nf1, Pten, Apc, Arid1a*). It was found that *Ovgp1-iCreER^{T2}* mice carrying different combinations of floxed genes develop HGSC-like oviductal tumors after transient treatment with tamoxifen [8]. Specifically, we generated mice targeted for loss of *Brca1, Trp53,* and *Rb1* (*BPR*); *Brca1, Trp53, Rb1* and *Nf1* (*BPRN*); *Brca1, Trp53* and *Pten* (*BPP*); *Apc* and *Pten* (*AP*); and *Apc, Pten,* and *Arid1a* (*APA*).

Figure 1 shows an example of the typical progression of the disease in *BPRN, BPR* and *BPP* mice as seen by formation of serous tubal intraepithelial carcinomas

(STIC) which progress to HGSC or its variant Malignant Mixed Mullerian Tumor (MMMT), and later metastasize to other regions [9].
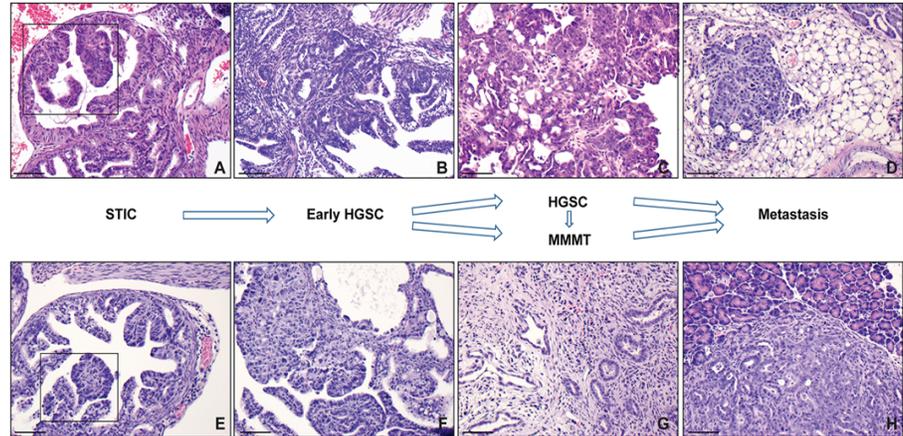

Figure 1: Typical progression of oviductal HGSC as seen in the mouse

To help determine how closely our mouse models recapitulate the molecular features of human HGSC, we performed targeted exome next generation sequencing (NGS) on a large number of oviductal tumors arising in our mice [10]. A list of the most commonly mutated genes found in human HGSC is provided in Table 1 [11]. We created

Trp53	Rb1	Nras	Pten
Brca1	Crebbp	Ccne1	Zmynd8
Csmd3	Smarcb1	Mecom	Irf2bp2
Nf1	Itgb7	Myc	Id4
Cdk12	Erbb2	Alg8	Pax8
Fat3	Acvr2b	Mettl17	Tert
Gabra6	Pdap1	Mycl	Map2k3
Brca2	Kras	Mcl1	Pik3ca

Table 1: Genes frequently mutated in human HGSCs identified by large scale sequencing and copy number analysis (TCGA)

a targeted exome panel to sequence the mouse homologs of these genes in tumor and normal samples from our various oviductal cancer models.

Materials and Methods

Genotyping of Mouse Samples

Polymerase chain reaction (PCR) using allele specific primers was performed to confirm the presence of desired engineered alleles (normal tail DNA) in each mouse and to confirm inactivation of engineered alleles in tumor DNA. PCR products were analyzed by conventional gel electrophoresis.

Mouse Tissue Histopathology

Tissues from euthanized mice were fixed in formalin and embedded in paraffin. The oviducts and ovaries were then serially sectioned in their entirety. 5 μm sections were cut using a microtome and mounted on glass slides. Alternate sections were stained with hematoxylin and eosin (H&E) in order to visualize any cancerous lesions in the tissue. H&E stained slides were then used as guides for selecting the particular areas of interest in the tissues from which DNA was isolated.

Immunohistochemical staining of mouse tissues

Alternate sections that were not stained with H&E were routinely saved for immunohistochemical (IHC) staining as seen in Figure 6. IHC was used to confirm up- or down-regulation of selected genes that were shown to have copy number alterations (e.g., amplification or deletion) according to the NGS results. Antigen retrieval was performed by microwaving the slides in citrate buffer (pH 6.0; Biogenex, San Ramon, CA) for 15 minutes. Endogenous peroxidase activity was quenched with 6% hydrogen peroxide in methanol. Staining was visualized with 3,3′-diaminobenzidine tetrahydrochloride and counterstaining with haematoxylin. Primary antibody used was

rabbit anti-PTEN (138G6/cat#9559, 1:400, Cell Signaling Technology, Inc., Danvers, MA).

Isolation of DNA and RNA from Formalin-Fixed Paraffin Embedded (FFPE) Tissues

The Qiagen AllPrep FFPE DNA/ RNA kit was used to isolate DNA and RNA from the tumor and normal samples. This multistep process allows for simultaneous DNA and RNA isolation through a series of washes and elution. Using a spectrophotometer, DNA and RNA were analyzed after running a blank as a control, and each sample's concentration and quality were measured. Because our samples were isolated from FFPE tissues, the quality and quantity of nucleic acid was quite variable. Often, there was a very low concentration of DNA or there had been degradation over time. When necessary, processing of samples was modified to ensure that there would be as high a quality of DNA as possible. Specifically, sections of the paraffin embedded samples were cut slightly thicker (10 μm) or multiple slides made from a particular sample were used when the tumors were especially small from which DNA was being isolated. Ultimately, sufficient quantities of purified DNA and RNA were obtained from each sample.

Targeted exome Next Generation Sequencing (NGS) of normal and tumor DNA samples

In order to analyze DNA alterations in the tumors arising in our various genetically engineered mouse models of oviductal cancer, we performed multiplexed PCR-based NGS from 15 normal and 81 tumor DNA samples. Dr. Scott Tomlins (University of Michigan Department of Pathology) and his lab were instrumental in providing the tools

for this analysis and assisting with the data analysis. Specifically, Tomlins designed a custom Ampliseq panel (1,445 amplicons targeting ~144kb) targeting the complete coding sequence of the mouse homologs of the 32 most significantly mutated (oncogenic and deleterious) and amplified/deleted genes in human HGSCs based on The Cancer Genome Atlas (TCGA) as shown in Table 1 [10]. Barcoded, mxNGS libraries were generated from 20 ng DNA per tumor, using this custom mouse Ampliseq panel and the Ion Ampliseq Library kit 2.0; sequencing was performed on an Ion Torrent Proton sequencer as described [11]. The data generated by targeted NGS can identify somatic or inherited mutations such as point mutations, small insertions or deletions, and copy number alterations (CNAs). 1445 amplicons were targeted and 96 samples were sequenced, 94 of which passed the library QC metrics (14 normal, 80 tumor).

Results

In order to confirm the genotypes of mice included in this analysis, allele specific PCR was used to verify the presence of the desired floxed alleles in tail DNA and Cre-mediated recombination of these alleles in matched tumor DNA. An example of such an analysis is shown in Figure 2. This particular example shows that in mice carrying one floxed and one wild type *Rb1* allele, matched tumors often show deletion of the wild type allele in addition to recombination of the floxed allele.
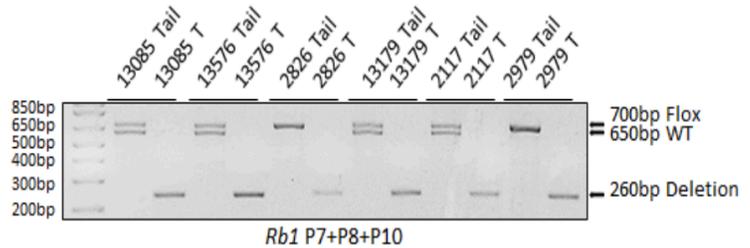

Figure 2: Example of PCR analysis confirming the successful genetic engineering of floxed and deleted Rb1 alleles in mouse tumor samples paired with their respective tail DNA

Targeted exome NGS sequencing was performed on DNA samples isolated from 14 normal and 80 tumor samples (51 *BPRN*, 4 *BPR*, 5 *BPN*, 12 *BPP*, 4 *AP,* and 4 *APA*). In some cases, more than one tumor sample was obtained from a single mouse (e.g., right and left oviductal tumors, metastatic tumor). We performed somatic copy number profiling from the mouse samples based on NGS data for the genes shown in Table 1. Notably, these genes are widely distributed throughout the mouse genome, including 15 of the 19 mouse autosomes.

Figure 3 shows examples of amplicon sequencing data from representative tumors arising in *BPRN* mice (Figures 3A and 3B) and from normal tissue (Figure 3C). Since *BPRN* mice have floxed alleles of *Brca1, Trp53, Rb1* and *NF1,* the tumors show deletions of the expected regions of each of these genes (boxed regions). These deletions are not observed in normal tissue from a *BPRN* mouse. In addition to

widespread copy number gains and losses not seen in the normal tissue sample, the
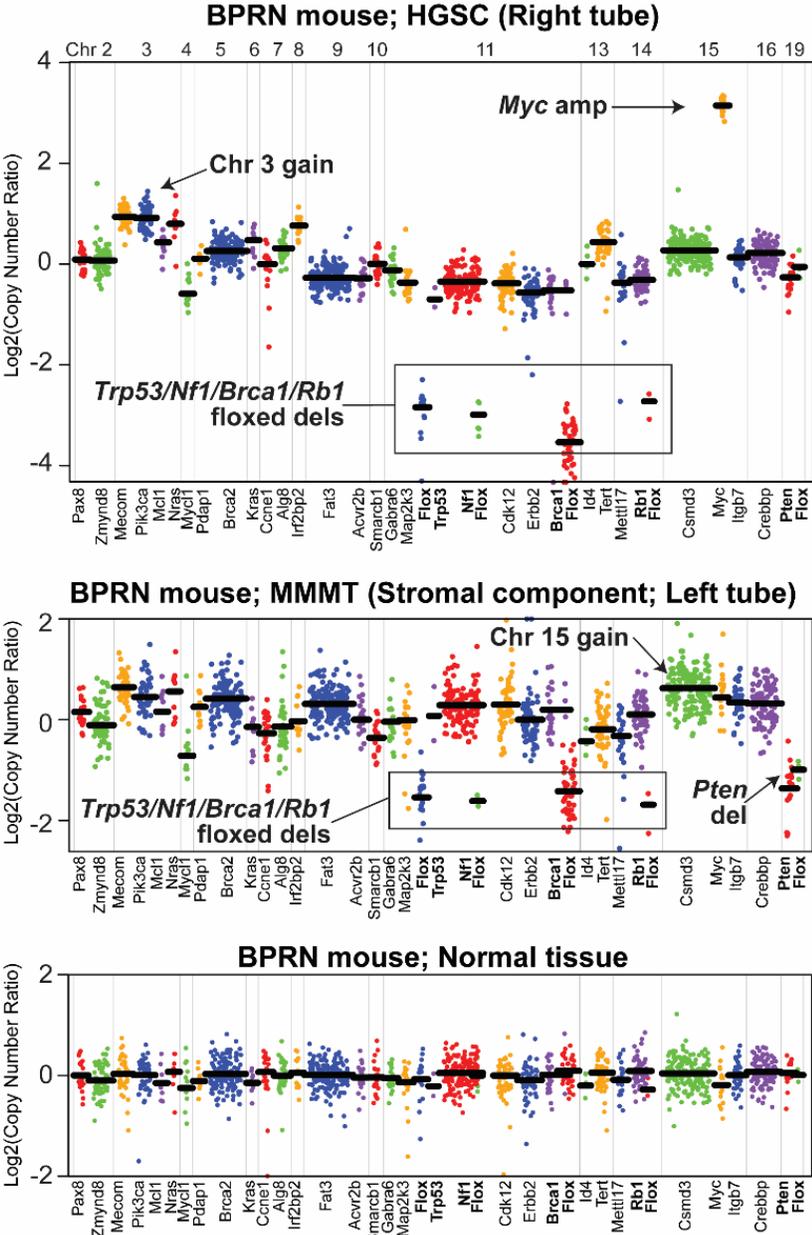

Figure 3: DNA copy number alterations in representative tumor and normal tissue samples. (A) Tumor from *BPRN* mouse shows amplification of *Myc* and chromosome 3 gain. (B) Tumor from a different *BPRN* mouse shows gain of chromosome 15 and deletion of *Pten* (C) a normal tissue sample with mean bars around 0 indicating no DNA copy number alterations. Sequenced genes are shown at bottom of each panel and each amplicon is represented by a colored dot. Floxed regions are shown separately from the non-floxed region of engineered genes.

tumors acquire other somatic alterations observed in a subset of human HGSCs, such as high-level amplification of *cMyc* (Figure 3A) and biallelic deletion of *Pten* (Figure 3B).

Importantly, widespread copy number alterations are a hallmark of human HGSCs that is recapitulated by tumors arising in our genetically engineered mice. Unsupervised hierarchical clustering of the CNA profiles was performed, in which samples with more similar CNA profiles are grouped together. The data from each mouse and all of
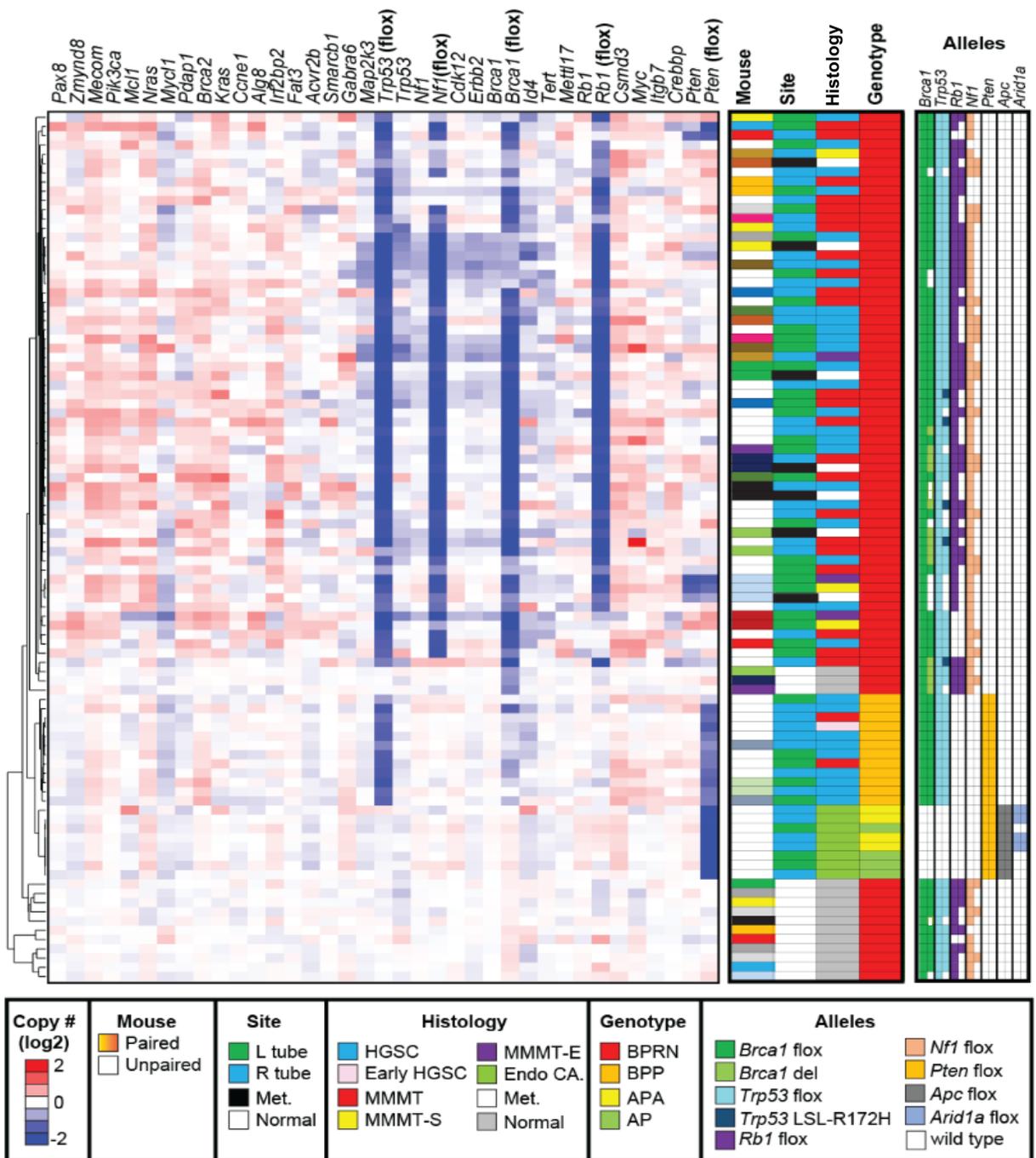
Figure 4: Heat map generated by NGS showing amplifications and deletions of targeted genes. 94 samples are shown in the map and 32 genes were analyzed

the genes analyzed were compiled into a large scale heat map shown in Figure 4.

From right to left, columns show the specific engineered alleles possessed by each

mouse, abbreviated genotype (i.e., *BPRN, BPP, AP, APA*), type of lesion histology, site

of the tumor or normal sample, and which samples are from the same mouse as coded by color.

In the heat map, copy number gains are indicated in red and losses in blue with color intensity reflecting the magnitude of gains and losses. The *BPRN* mice are clustered together and show obvious blue regions corresponding to deletions of the floxed portions of *Brca1, Trp53, Rb1* and *Nf1. BPP* mice also cluster together and show deletion of floxed portions of *Brca1, Trp53* and *Pten.* Tumors with deletions of *Apc, Pten, +/- Arid1a* also cluster together (*AP* and *APA*).

Finally, there are 2 different groups of normal samples which are identified by the gray colored boxes under the histology column. While at first the separation of the two normal groups was unexpected, the 3 that were grouped apart from the other normal samples have a germline deletion of *Brca1* and cluster more closely to the *BPRN* tumors than to the other normal tissues based on CNA profile. This distinction helps to validate the unsupervised nature of the cluster analysis. Additional genes that were deleted or amplified in the tumor samples can be seen by blocks of deep red or blue that appear in several other areas that were not specifically targeted by Cre-recombinase.

Interestingly, we noticed that there were a number of samples in the *BPRN* group with a reduction in *Pten* gene copy number even though we did not target *Pten* for deletion in these mice. In order to confirm these results, PCR was performed to verify *Pten* loss in the tumor samples compared to matched normal samples. Figure 5 shows that the band corresponding to the wild type allele of Pten that was clearly present for the normal samples is absent in the paired tumor samples. The 14433 samples were

isolated from a mouse that was engineered to be heterozygous for *BPRN*, meaning there was one floxed allele of each *Brca1, Trp53, Rb1* and *Nf1* and the other was a wild type allele (Supplemental Figure S1).
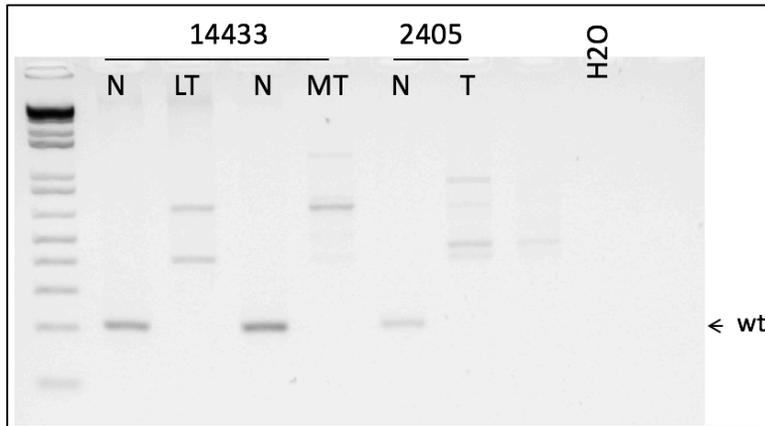

Figure 5: PCR of normal tissue samples paired with tumor samples in selected *BPRN* mice showing *Pten* loss. For sample 14433, LT indicates a tumor isolated from the left oviduct and MT indicates tumor isolated from a metastasis. Sample 2405 showed presence of *Pten* allele in normal tissue compared to the tumor. Water (no DNA) was used as a negative control.

The data shown in Figure 5 confirm deletion of *Pten* in the tumor and metastasis samples (non-specific bands appear in the lanes corresponding to the tumor samples). Mouse 2405, was engineered with genotype $Brca1^{flox/flox}$, $Trp53^{flox/flox}$, $Rb^{+/+}$, $Nf1^{flox/+}$ (Supplemental Figure S1). Like the tumors arising in mouse 14433, wild type *Pten* was deleted in the tumor sample from mouse 2405.

To further confirm deletion of *Pten* in the tumor samples from mice 14433 and 2405, expression of PTEN protein was analyzed using IHC staining (Figure 6). Figure 6A shows loss of PTEN expression in a tumor from an *APA* mouse with confirmed deletion of *Pten*. A section of a tumor from an *BPP* mouse is stained in Figure 6B. Figure 6C shows PTEN IHC staining of a *BPRN* tumor with somatic deletion of *Pten* while a tumor without *Pten* deletion that retained normal expression of PTEN is shown in Figure 6D. These data show that tumors with somatic deletion of *Pten* lose expression of PTEN protein, a feature often seen in human HGSCs [12].
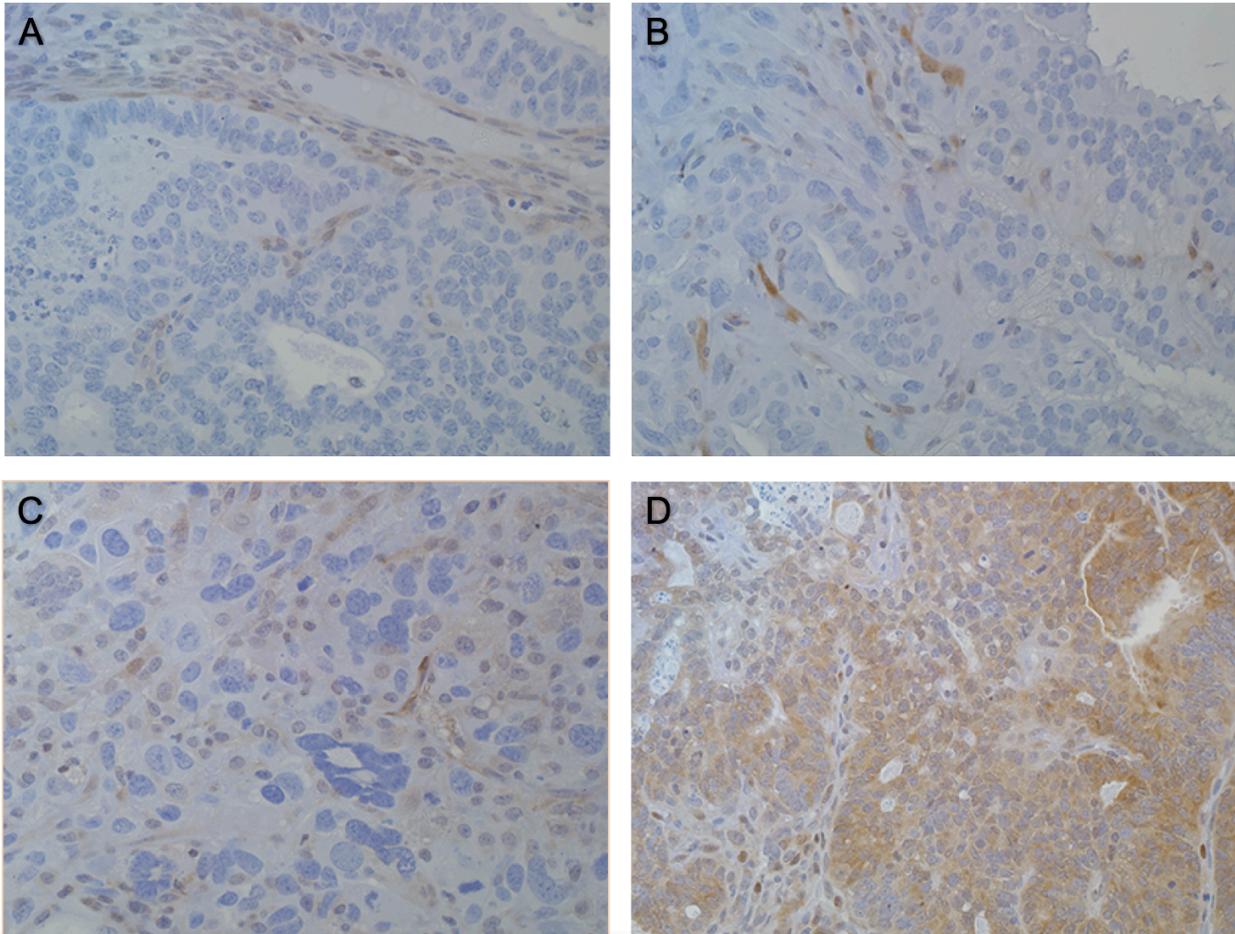
Figure 6: Immunohistochemical staining for PTEN expression. (A) shows a representative section of a tumor from an *APA* mouse #14593 in which the *Pten* allele was targeted for deletion and shows little positive staining for the protein. (B) is a section from a *BPP* mouse #15073 which was also targeted for *Pten* deletion and also shows little positive staining. (C) is a section from tumor of *BPRN* mouse #14433 that showed copy number losses of *Pten* and (D) is a positive control mouse #14396.

In addition, according to the heat map, *Myc* was seen to have increased copy numbers in several BPRN mice. Again, even though we did not genetically manipulate the mice with regard to the *Myc* gene, the genetic instability of *BPRN* mice resulted in further mutations causing the loss of additional genes. The human model of HGSC follows the same pattern and tends to acquire additional copies of *Myc* resulting in upregulation [13].

The NGS data also showed partial, rather than complete, Cre-mediated deletion of *Brca1* in most of the tumors arising in mice carrying homozygous floxed *Brca1,*
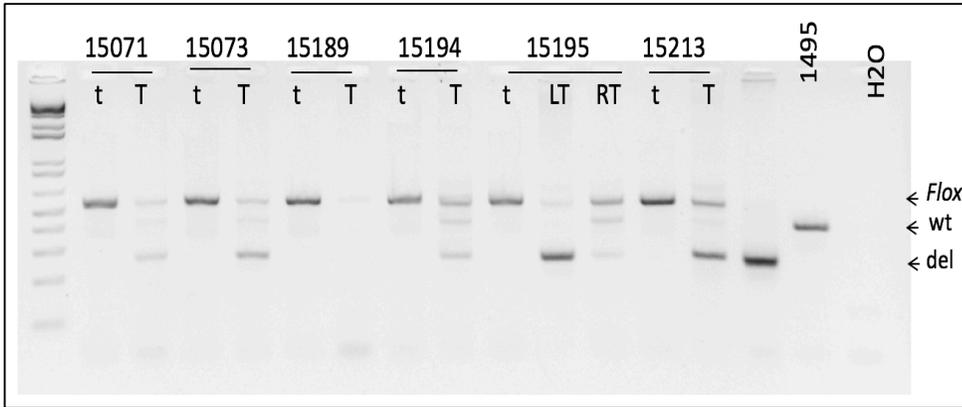
Figure 7: PCR analysis of tail (t) DNA paired with tumor (T) DNA from *BPP* mice. Primers were used to detect floxed, wild type or deleted *Brca1* alleles in these samples. LT and RT represent left and right tumors from mouse 15195.

Trp53, and *Pten* alleles (*BPP* mice) which was unexpected. In order to confirm the results seen in the heat map (Figure 4), PCR was performed to analyze the status of the floxed *Brca1* alleles in tissues from representative *BPP* mice. Figure 7 shows the PCR analysis of *Brca1* status in DNA isolated from representative tumors arising in *BPP* mice (Supplemental Figure S2) compared to their corresponding tail DNA. In these cases, PCR of tail DNA confirmed the presence of only floxed *Brca1* alleles. However, in the tumor samples there was incomplete deletion of *Brca1*.

Discussion

The purpose of this research was to test how well mouse models of HGSC match to the molecular features of HGSCs arising in humans. Mouse models that closely mimic their human counterparts can be used to test new strategies for early detection and prevention of HGSC.

Mice were first analyzed in order to see which combinations of inactivated genes would lead to oviductal tumors. They were placed into categories including *BPP*, *BPN*, or *BPRN* depending on the genes targeted for floxed deletion. These data were used to select tumor samples from lesions in paired oviducts, as well as from metastases regions, while comparing them to controls. The samples were then subjected to NGS to measure copy number changes of the 32 most commonly mutated genes in HGSC [10]. HGSC, like other cancers, results in genetic instability in both human and mouse models. As predicted, this was seen in the results of the NGS data by widespread alterations to copy numbers in these genes of interest.

Figure 4 indicates widespread deletions of the floxed genes in *BPRN* mice which cluster together on the chart. It also shows a significant clustering of *BPP*, *APA,* and normal samples. The *BPP* and *APA* mice also show that the targeted regions were deleted as expected, as seen by dark bands of blue corresponding to copy number loses in those cases. The data also show that tumors from these mice acquired additional changes that coincide with data observed in human HGSCs, including amplification of *cMyc* and deletion of *Pten*.

The deletion of *Pten* was first confirmed with PCR. As shown in Figure 5, a *BPRN* mouse, 14433, appeared to have spontaneously lost the *Pten* gene in the tumor

and metastases samples since there is no band corresponding to the wild type allele of the gene. Comparing this to the sample of normal tissue, however, it is clear that this was a specific deletion acquired by only the cancerous regions. The normal sample retained the band for *Pten*. In addition, mouse 2405, which was categorized as *BPN,* appeared to also have lost copies of *Pten* according to the heat map. Once again, a comparison of the tumor to a normal tissue sample from the mouse confirmed the presence of the wild type allele only in the normal sample and was lacking in the tumor sample.

Furthermore, IHC staining was done to look at the expression of the gene. Figure 6 shows representative sections from 4 different mice: 6A an *APA* mouse, 6B a *BPP* mouse, 6C a *BPRN* mouse identified as having lost copies of *Pten* according to the heat map, and 6D a positive control with known *Pten* expression. Since *Pten* had been targeted for deletion in both the *APA* mouse as well as the *BPP* mouse, it was predicted that there would be very little positive staining in these two samples. Figure 6C was a sample derived from the same mouse that was checked with PCR for loss of *Pten.* Since this sample too showed very little staining compared to the positive control, the data from the heat map were corroborated demonstrating that even in samples that were not targeted for *Pten* deletion, the tumors selected for cells with less copies of this gene. Thus the mouse HGSCs followed the same pattern as human HGSCs and the tumors were found to have spontaneously lost copies of this gene. This adds to the conclusion that our mouse model of HGSC does indeed correlate with the genetic profile and progression of the human model.

Another area of the interest on the heat map was where the *BPP* mice clustered. The samples showed a surprisingly weak loss of *Brca1* even though it was targeted for deletion for Cre recombinase. Figure 7 shows the confirmation of this incomplete deletion by PCR analysis. DNA from *BPP* tumors (T) as well as DNA from the mouse tail DNA (t) were compared using primers specific for *Brca1*. Again confirming the results of the heat map, bands from the tumors appeared that corresponded to the wild type, floxed and deleted alleles. By contrast, normal DNA from the same mice appeared to only have bands corresponding to floxed portions of the gene—which is expected since Cre recombinase targeted the oviducts for *Brca1* deletion. We conclude that since *Brca1* deletion is not strongly selected for in *BPP* mice, the loss of this gene is not necessary for tumor formation. In our *BPP* model system, deletion of *Pten* and *Trp53* appears to be sufficient to drive tumorigenesis.

Understanding which genes are mutated, and when, may allow for earlier HGSC diagnosis. For example, detection of tumor-specific DNA in routine Pap smears from women at high risk for developing HGSC could be used as an early detection strategy. Moreover, if tumor DNA is detected, the chances of metastasis could be determined based on knowledge of the general progression of the disease accompanied by accumulation of genetic mutations. Additional experiments will provide opportunities to explore these options and hopefully improve care for patients diagnosed with ovarian cancer.

Acknowledgements

First and foremost, thank you to Dr. Kathleen Cho and Dr. Yali Zhai who allowed me to do this research over the past two years. It has been an amazing opportunity to work alongside such brilliant minds and I'm grateful for your guidance. I've learned and grown so much as a student and a scientist.

Thank you to my friends who have encouraged me.

Thank you to my grandparents for inspiring me to work hard to reach my goals.

Thank you to my parents for your unconditional love and support.

References

1. Piek, J. M., van Diest, P. J., Zweemer, R. P. et al. (2001). Dysplastic changes in prophylactically removed Fallopian tubes of women predisposed to developing ovarian cancer. The Journal of pathology, 195(4), 451-456.

2. Vogelstein, B., Kinzler, K. (2004). Cancer genes and the pathways they control. Nature Medicine, 10(8), 789-799. doi:10.1038/nm1087

3. Wei, W., Dizon, D., Vathipadiekal, V. & Birrer, M. (2013). Ovarian cancer: genomic analysis. Annals Of Oncology, 24 (suppl 10), x7-x15. doi:10.1093/annonc/mdt462

4. Bowtell, D. D., Böhm, S., Ahmed, A. A. et al. (2015). Rethinking ovarian cancer II: reducing mortality from high-grade serous ovarian cancer. Nature reviews Cancer, 15 (11), 668.

5. Kindelberger, D. W., Lee, Y., Miron, A. et al. (2007). Intraepithelial carcinoma of the fimbria and pelvic serous carcinoma: evidence for a causal relationship. The American journal of surgical pathology, 31(2), 161-169.

6. Wu, R., Zhai, Y., Kuick, R., Karnezis, A. N. et al. (2016). Impact of oviductal versus ovarian epithelial cell of origin on ovarian endometrioid carcinoma phenotype in the mouse. The Journal of pathology, 240(3), 341-351.

7. Sauer, B. (1998). Inducible gene targeting in mice using the Cre/*lox* system. Methods, 14(4), 381-392.

8. Zhai, Y., Wu, R., Kuick, R., Sessine, M. S., Schulman, S., Green, M., ... & Cho, K. R. (2017). High-grade serous carcinomas arise in the mouse oviduct via defects linked to the human disease. The Journal of pathology.

8. Li, H. X., Lu, Z. H., Shen, K. et al. (2014). Advances in serous tubal intraepithelial carcinoma: correlation with high grade serous carcinoma and ovarian carcinogenesis. International journal of clinical and experimental pathology, 7(3), 848.

9. McDaniel, A. S., Stall, J. N., Hovelson, et al. (2015). Next-generation sequencing of tubal intraepithelial carcinomas. JAMA oncology, 1(8), 1128-1132.

10. Cancer Genome Atlas Research Network. (2011). Integrated genomic analyses of ovarian carcinoma. Nature, 474(7353), 609.

11. de la Vega, L. L., McHugh, J. B., Cani, A. K. et al. (2017). Comprehensive Molecular Profiling of Olfactory Neuroblastoma Identifies Potentially Targetable FGFR3 Amplifications. Molecular Cancer Research, 15(11), 1551-1557.

12. Perets, R., Wyant, G., Muto, K. et al. (2013). Transformation of the Fallopian Tube Secretory Epithelium Leads to High-Grade Serous Ovarian Cancer in Brca;Tp53;Pten Models. Cancer Cell, 24(6), 751-765. doi:10.1016/j.ccr.2013.10.013

13. Baker, V. V., Borst, M. P., Dixon, D. et al. (1990). C-myc amplification in ovarian cancer. Gynecologic oncology, 38(3), 340-342.

Supplemental Figures

	Mouse ID	Oviductal Lesion R	Oviductal Lesion L	Months at Death	*Brca1*		*Trp53*		*Rb1*		*Nf1*		Peritoneal Metastasis	Matched normal tissue
1	3867		MMMT	13.5									+	+
2	14286		HGSC	15.5										
3	13735		MMMT	9										
4	13604	HGSC		12									+	+
5	2769	HGSC	MMMT	14.5									+	+
6	2979	MMMT		13										
7	13238	HGSC		15										
8	2611	HGSC	MMMT	15.5									+	+
9	14154		MMMT	12.5										+
10	14390	MMMT		11.5										
11	14396	MMMT		13.5										
12	2942	HGSC		15.5										
13	13311	MMMT		18.5										
14	13268	HGSC		18.5										
15	14150		MMMT	16										
16	14085	MMMT		13.5										
17	14806		MMMT	14.5										
18	14109		HGSC	13										
19	13375	MMMT		13.5										
20	2778		MMMT	22.5										+
21	14104		HGSC	15.5										+
22	14526	MMMT		15.5									+	
23	14174	MMMT		16										
24	14280	HGSC		17										
25	3694		HGSC	19.5										
26	8234		HGSC	19.5										
27	13179	HGSC		13										
28	3807	MMMT		22.5										
29	14397	MMMT	HGSC	16.5										
30	14474	MMMT		16										+
31	13085	HGSC		12.5										
32	13576	HGSC		13.5										
33	2163		HGSC	16										
34	14399	MMMT		14									+	
35	14059	MMMT		17										
36	14120	MMMT		18										
37	14433		MMMT	17.5									+	+
38	2285		MMMT	19.5										
39	2519	HGSC	MMMT	19.5										+
40	2016		HGSC	27										
41	3695	HGSC		22										
42	14270		HGSC	18										
43	2027		MMMT	26										
44	2405	HGSC	MMMT	24										+

Legend:
- MMMT
- HGSC
- Early HGSC
- STIC
- Lesions not detected
- R: right
- L: left
- *Brca1*^{flox}
- *Brca1*^{del}
- *Trp53*^{flox}
- *Trp53*$^{LSL-R172H}$
- *Rb1*^{flox}
- *Nf1*^{flox}

Supplemental Figure S1: DNA samples from Oviductal Tumors in TAM-treated *BPRN, BPR* and *BPN* mice for targeted sequencing.

	Mouse ID	Oviductal Lesion		Months post-TAM	Brca1		Trp53		Pten	
		R	L							
1	14721	🟥		4						
2	14943		🟥	8						
3	15071	🟨		7						
4	15073	🟦		7						
5	15189		🟦	8						
6	15191	🟦		8						
7	15194	🟦		7.5						
8	15195	🟦		8						
9	15213	🟦		8						
10	15217		🟦	7						

Legend:
- 🟩 Brca1 flox
- 🟦 Trp53 flox
- 🟧 Pten flox

Supplemental Figure S2: Summary of Oviductal Tumor Phenotype in TAM-treated *BPP* mice